Applied Catalysis B: Environmental 144 (2014) 521–527

Contents lists available at ScienceDirect

Applied Catalysis B: Environmental

journal homepage: www.elsevier.com/locate/apcatb

MoS_2 as non-noble-metal co-catalyst for photocatalytic hydrogen evolution over hexagonal $ZnIn_2S_4$ under visible light irradiations

Liang Wei, Yongjuan Chen, Yiping Lin, Haishan Wu, Rusheng Yuan, Zhaohui Li*

Research Institute of Photocatalysis, Fujian Provincial Key Laboratory of Photocatalysis-State Key Laboratory Breeding Base, College of Chemistry and Chemical Engineering, Fuzhou University, Fuzhou 350002, PR China

A R T I C L E I N F O

Article history:
Received 14 May 2013
Received in revised form 23 July 2013
Accepted 28 July 2013
Available online 7 August 2013

Keywords:
MoS_2
Co-catalyst
Photocatalytic
Hydrogen evolution
Visible light

A B S T R A C T

$MoS_2/ZnIn_2S_4$ nanocomposites were prepared by impregnating the hydrothermally prepared hexagonal $ZnIn_2S_4$ microspheres with an aqueous solution of $(NH_4)_2MoS_4$, followed by a treatment in H_2S flow at high temperatures to transform Mo(VI) to Mo(IV). The as-prepared $MoS_2/ZnIn_2S_4$ nanocomposites were characterized by X-ray diffraction (XRD), Raman spectroscopy, X-ray photoelectron spectroscopy (XPS), transmission electron microscopy (TEM) and high-resolution transmission electron microscopy (HRTEM). Their photocatalytic performance for hydrogen evolution under visible light irradiations was also investigated. It was found that the photocatalytic hydrogen evolution activity over hexagonal $ZnIn_2S_4$ can be significantly increased by loading MoS_2 as a co-catalyst and the photocatalytic activity of $MoS_2/ZnIn_2S_4$ nanocomposites could be even higher than that of $Pt/ZnIn_2S_4$ under similar reaction condition. Amorphous MoS_2 was for the first time shown to exhibit excellent promoting effect for photocatalytic hydrogen evolution. The promoting effect played by amorphous MoS_2 can be ascribed to the existence of many defect sites in amorphous MoS_2 which can act as adsorption sites for hydrogen atoms and eventually leads to hydrogen evolution. This work demonstrates a high potential of the developing of environmental friendly, cheap noble metal-free co-catalyst for semiconductor-based photocatalytic hydrogen evolution.

© 2013 Elsevier B.V. All rights reserved.

1. Introduction

Hydrogen is a clean and green fuel. The conversion and store solar energy in the form of hydrogen by photocatalytic water splitting holds great promise to meet the future energy and environment requirement [1–4]. Ever since the initial study of a photoelectrochemical cell using $Pt–TiO_2$ electrodes for hydrogen evolution by Fujishima and Honda in 1972, great efforts have been devoted to the development of highly efficient semiconductor photocatalysts for H_2 production [5]. So far, a variety of active photocatalysts for H_2 production, including metal oxides [6–8], sulfides [9,10] and oxynitrides [11,12], have already been developed. Among the numerous types of semiconductor systems studied, metal sulfides have demonstrated promising activities toward H_2 production from water containing sacrificial reagents under visible light. $ZnIn_2S_4$ is a ternary chalcogenide which has a suitable band gap (2.34–2.48 eV) well corresponding to the visible light absorption. $ZnIn_2S_4$ exhibits two distinct polymorphs based on cubic and hexagonal lattices. Previous studies have revealed that both polymorphs of $ZnIn_2S_4$ are active for photocatalytic H_2 generation under visible light irradiations and show considerable chemical stability [13–16]. However, the photocatalytic H_2 evolution activity over bare $ZnIn_2S_4$ is low because of the short lifetimes of the photogenerated electron–hole pairs. Co-catalyst like Pt should be loaded onto $ZnIn_2S_4$ to enhance the photocatalytic H_2 production activity of $ZnIn_2S_4$.

Studies on semiconductor-based photocatalysts revealed that co-catalysts loaded on the surface of semiconductor photocatalysts play important roles in promoting their photocatalytic performance. An appropriate co-catalyst can suppress the recombination of the photo-generated charge carriers, lower the over potential for hydrogen evolution and also provide redox reaction sites for H_2 evolution to avoid back reactions. Due to their negligible overpotential for H_2 evolution and excellent kinetics for driving the hydrogen evolution reaction (HER), noble metals like Pt [17,18], Rh [19], Au [20–22] and their oxides like RuO_2 [23], $Rh_xCr_{2-x}O_3$ [24] are generally used as the co-catalysts for photocatalytic hydrogen evolution. However, the precious metals are expensive and to reduce the cost of renewable H_2 production, it is necessary to explore alternative co-catalysts based on inexpensive transition metals.

Recently transition metal sulfides like MoS_2 [25–28], WS_2 [29] and NiS [30] have been demonstrated to be excellent co-catalyst for CdS and TiO_2 in the photocatalytic hydrogen evolution. Among

* Corresponding author. Tel.: +86 591 83779260; fax: +86 591 83779260.
E-mail addresses: zhaohuili1969@yahoo.com, zhaohuili@fzu.edu.cn (Z. Li).

0926-3373/$ – see front matter © 2013 Elsevier B.V. All rights reserved.
http://dx.doi.org/10.1016/j.apcatb.2013.07.064

these transition metal sulfide co-catalysts, MoS_2 nanomaterial has received a lot of attention since it is a good electrocatalyst for H_2 evolution, and its HER activity stemmed from the sulfur edges of the MoS_2 crystal layers [31]. MoS_2 has an intrinsic layered structure consisting of S–Mo–S sheets held together in stacks by van der Waals interactions. Dai et al. [32] reported that nano-structured MoS_2 grown on RGO exhibited excellent HER activity due to its high exposure of the edges and its strong electronic coupling with the underlying RGO. Recently, MoS_2 grown on g-C_3N_4 is demonstrated to show high activity for photocatalytic hydrogen evolution due to the formation of the layered nanojunction between MoS_2 and g-C_3N_4 [33].

Similar to g-C_3N_4, hexagonal $ZnIn_2S_4$ has an intrinsic layered structure based on a stacking of packets of S–Zn–S–In–S–In–S layers. It is expected that it is facile to grow layer MoS_2 on hexagonal $ZnIn_2S_4$ surface due to their analogous layered structures which can minimize the lattice mismatch. Besides this, the position of the conduction band of MoS_2 lies between −0.5 and −0.9 vs. NHE according to their dimension based on the study by Thurston and Wilcoxon [34]. The conduction band position of MoS_2 is less negative as compared to that of hexagonal $ZnIn_2S_4$ (−1.1 eV vs. NHE) and thus provides possibility for a directional transfer of the photogenerated electrons from $ZnIn_2S_4$ to MoS_2. Moreover, the electrons transferred to the conduction band of MoS_2 can still maintain enough chemical potential to reduce H^+ to hydrogen at HER active sites of MoS_2. Therefore, it is supposed that MoS_2 can be an ideal candidate as a non-noble-metal co-catalyst for hexagonal $ZnIn_2S_4$ in photocatalytic H_2 evolution.

In this manuscript, we reported the preparation of $MoS_2/ZnIn_2S_4$ nanocomposites for photocatalytic hydrogen evolution under visible light irradiations. $MoS_2/ZnIn_2S_4$ nanocomposites were prepared by impregnating the hydrothermally prepared hexagonal $ZnIn_2S_4$ with an aqueous solution of $(NH_4)_2MoS_4$, followed by a treatment in H_2S flow at high temperatures. Their photocatalytic performance for hydrogen evolution was evaluated under visible light irradiations. It was found that the photocatalytic hydrogen evolution activity over hexagonal $ZnIn_2S_4$ can be significantly increased by loading MoS_2 as a co-catalyst. The photocatalytic activity of $MoS_2/ZnIn_2S_4$ can be even higher than that of $Pt/ZnIn_2S_4$ under similar reaction conditions.

2. Experimental

2.1. Preparations

All the reagents are analytical grade and used without further purifications. Hexagonal $ZnIn_2S_4$ powder was synthesized according to our previously reported method [14]. $(NH_4)_2MoS_4$ was prepared according to the literature and was used as precursor for MoS_2 to be loaded on $ZnIn_2S_4$ [35]. Different amounts of molybdenum species were loaded on $ZnIn_2S_4$ by an impregnation method from solution containing different amounts of $(NH_4)_2MoS_4$. After vacuum drying at 333 K for 6 h, $(NH_4)_2MoS_4/ZnIn_2S_4$ precursors were calcinated for 3 h at temperatures 623 and 723 K respectively in 10% H_2S–90% H_2 mixed gas atmosphere to obtain the $MoS_2/ZnIn_2S_4$ nanocomposites. Samples obtained at temperature 623 K and 723 K was denoted as $MoS_2/ZnIn_2S_4$-623 K and $MoS_2/ZnIn_2S_4$-723 K, respectively.

1.0 wt% $Pt/ZnIn_2S_4$ photocatalyst was prepared by a photodeposited method using $H_2PtCl_6 \cdot 6H_2O$ as the starting material. Pure MoS_2 sample (denoted as MoS_2-c) was obtained using $(NH_4)_2MoS_4$ as precursor and calcinated at 623 K in H_2S flow.

2.2. Characterizations

X-ray diffraction (XRD) patterns were collected on a Bruker D8 Advance X-ray diffractometer with Cu K_α radiation. Raman spectra were recorded with a confocal Raman micro-spectrometer (Renishaw, Great Britain) in the range of 500–2100 cm^{-1} under a 785 nm diode laser excitation. The spectra were collected in a backscattering geometry using a microscope equipped with a Leica 20× objective in a spectral resolution of 2 cm^{-1}. The detection of the Raman signal was carried out with a Peltier cooled charge-coupled device (CCD) camera. The software package WIRE 2.0 (Renishaw) was employed for acquisition and analysis. UV–visible diffraction spectra (UV–vis DRS) of the powders were obtained for the dry pressed disk samples using a UV–visible spectrophotometer (Cary 500 Scan Spectrophotometers, Varian). $BaSO_4$ was used as a reflectance standard. The transmission electron microscopy (TEM) and high-resolution transmission electron microscopy (HRTEM) images were measured by a JEOL model JEM 2010 EX instrument at an accelerating voltage of 200 kV. The powder particles were supported on a carbon film coated on a 3 mm diameter fine-mesh copper grid. A suspension in ethanol was sonicated and a drop was dripped on the support film. The morphology of the sample was characterized by field emission scanning electron microscopy (SEM) (JSM-6700F). X-ray photoelectron spectroscopy (XPS) measurements were performed on a PHI Quantum 2000 XPS system with a monochromatic Al K_α source and a charge neutralizer. All of the binding energies were referred to the C 1s peak at 284.8 eV of the surface adventitious carbon.

2.3. Photocatalytic H_2 evolution

Photocatalytic H_2 evolution experiments were carried out in a closed gas circulation and evacuation system fitted with a top Pyrex window. 50 mg of photocatalyst was dispersed in 100 ml of aqueous solution containing 0.5 M Na_2SO_3 and 0.43 M Na_2S as sacrificial reagents. The suspension was irradiated with a 300 W Xe lamp equipped with a 420 nm cutoff filter to provide the visible light irradiations. The temperature of the reactant solution was maintained at room temperature by a flow of cooling water during the photocatalytic reaction. The amount of H_2 evolved was determined with an on-line gas chromatography equipped with a TCD detector.

3. Results and discussion

$ZnIn_2S_4$ was prepared according to our previously reported method [14]. Since $(NH_4)_2MoS_4$ starts to decompose to form MoS_2 at 623 K, $MoS_2/ZnIn_2S_4$ nanocomposites were prepared by treating the $(NH_4)_2MoS_4/ZnIn_2S_4$ precursors at temperatures higher than 623 K in 10% H_2S–90% H_2 to obtain the $MoS_2/ZnIn_2S_4$ composites. Fig. 1 shows the X-ray diffraction patterns of $ZnIn_2S_4$ and 1.0 wt% $MoS_2/ZnIn_2S_4$ obtained at 623 and 723 K. As shown in Fig. 1b, 1.0 wt% $MoS_2/ZnIn_2S_4$-623 K shows 2θ peaks at values of 21.6°, 27.7°, 30.4°, 39.8°, 47.2°, 52.4° and 55.6°, which can be assigned to (0 0 6), (1 0 2), (1 0 4), (1 0 8), (1 1 0), (1 1 6) and (0 2 2) crystallographic planes of hexagonal $ZnIn_2S_4$ phase (JCPDS-03-065-2023). However, in addition to peaks corresponding to hexagonal $ZnIn_2S_4$, $MoS_2/ZnIn_2S_4$-723 K shows additional 2θ diffraction peaks at values of 27.0° and 27.9°, which can be assigned to (1 0 4) and (1 0 7) crystallographic planes of rhombohedral $ZnIn_2S_4$ phase, indicating that calcinating at 723 K partially transform the hexagonal $ZnIn_2S_4$ to rhombohedral one. In the XRD patterns of both samples, diffraction peaks assigned to MoS_2 were not observed, probably due to the low amount of MoS_2 and its high dispersion on $ZnIn_2S_4$.

The Raman spectroscopy studies were performed on the as-prepared $MoS_2/ZnIn_2S_4$ nanocomposites and were compared with

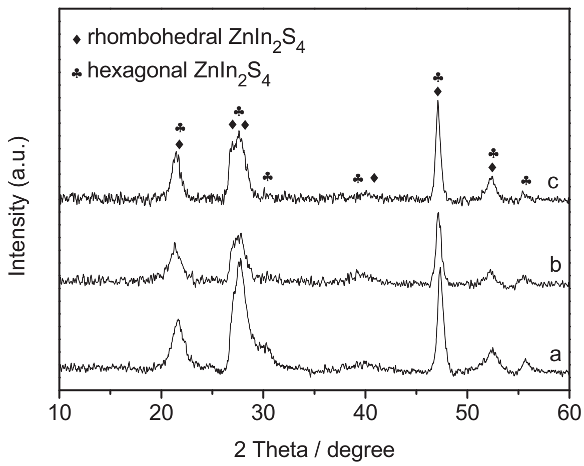

Fig. 1. XRD patterns of (a) bare $ZnIn_2S_4$; (b) 1.0 wt% $MoS_2/ZnIn_2S_4$-623 K; (c) 1.0 wt% $MoS_2/ZnIn_2S_4$-723 K. (♦) Rhombohedral $ZnIn_2S_4$; (♣) hexagonal $ZnIn_2S_4$.

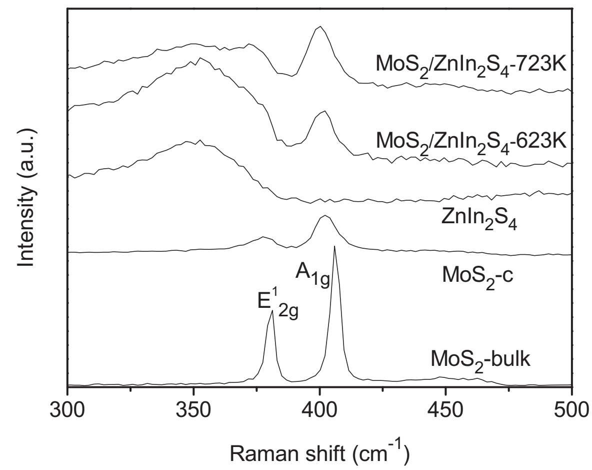

Fig. 2. Raman spectra of bulk MoS_2; MoS_2-c; bare $ZnIn_2S_4$; $MoS_2/ZnIn_2S_4$-623 K and $MoS_2/ZnIn_2S_4$-723 K.

that of bulk MoS_2, MoS_2-c and pure hexagonal $ZnIn_2S_4$. As shown in Fig. 2, in addition to the peaks corresponding to pure hexagonal $ZnIn_2S_4$, typical MoS_2 peaks at about 379 cm^{-1} arising from the in-plane $E^1{}_{2g}$ vibration and 401 cm^{-1} arising from the out-of-plane A_{1g} vibration were observed in both $MoS_2/ZnIn_2S_4$ nanocomposites obtained at different calcination temperature [36,37]. Similar to those observed over MoS_2-c, these bands in $MoS_2/ZnIn_2S_4$ nanocomposites are much broader than those observed over bulk MoS_2. Previous study found that the single-layer MoS_2 nanosheet exhibits much broader Raman bands relative to their bulk counterpart due to the phonon confinement in the ultra-thin structure [38]. The Raman results indicate that thin-layer MoS_2 has been successfully incorporated within $ZnIn_2S_4$.

XPS analyses were carried out on a typical $MoS_2/ZnIn_2S_4$ sample. The XPS spectrum of $MoS_2/ZnIn_2S_4$ in the Mo 3d region shows binding energy at 228.9 eV for Mo $3d_{5/2}$ and 231.9 eV for Mo $3d_{3/2}$

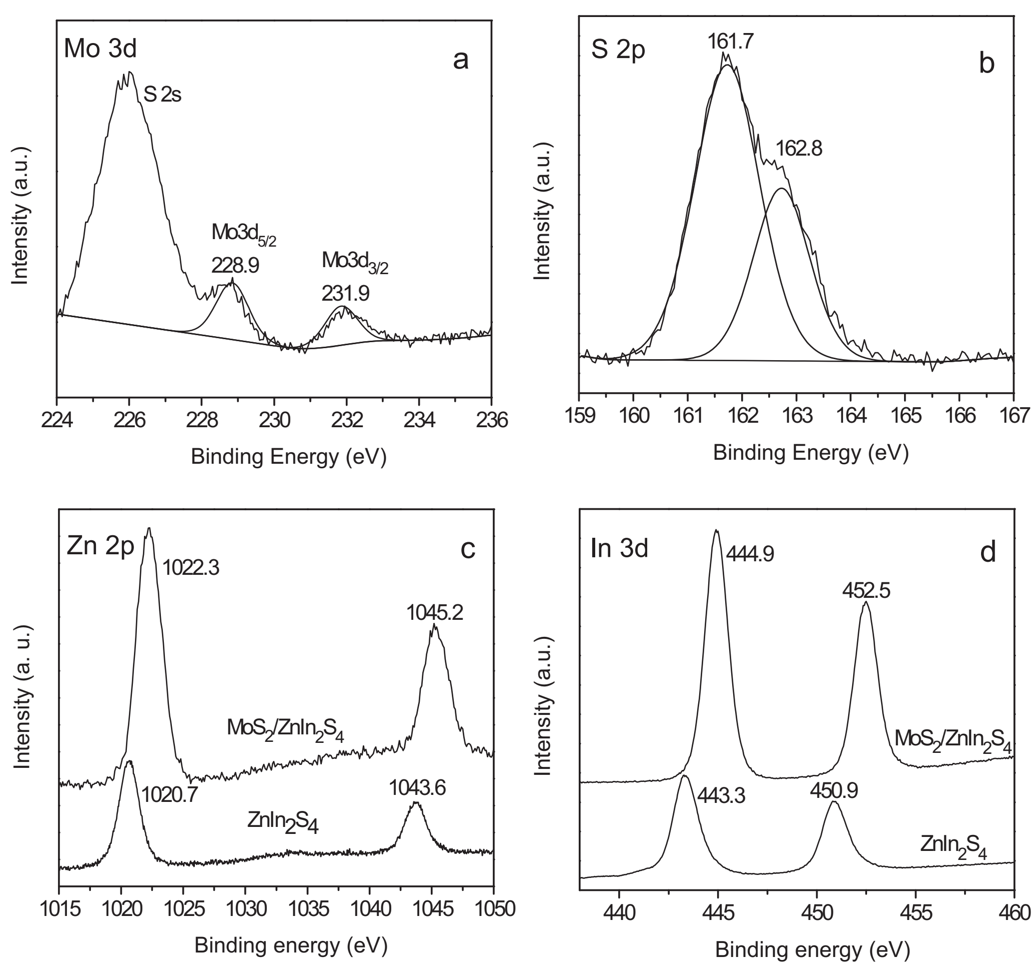

Fig. 3. XPS spectra of $MoS_2/ZnIn_2S_4$ and $ZnIn_2S_4$ (a) Mo 3d; (b) S 2p; (c) Zn 2p and (d) In 3d.

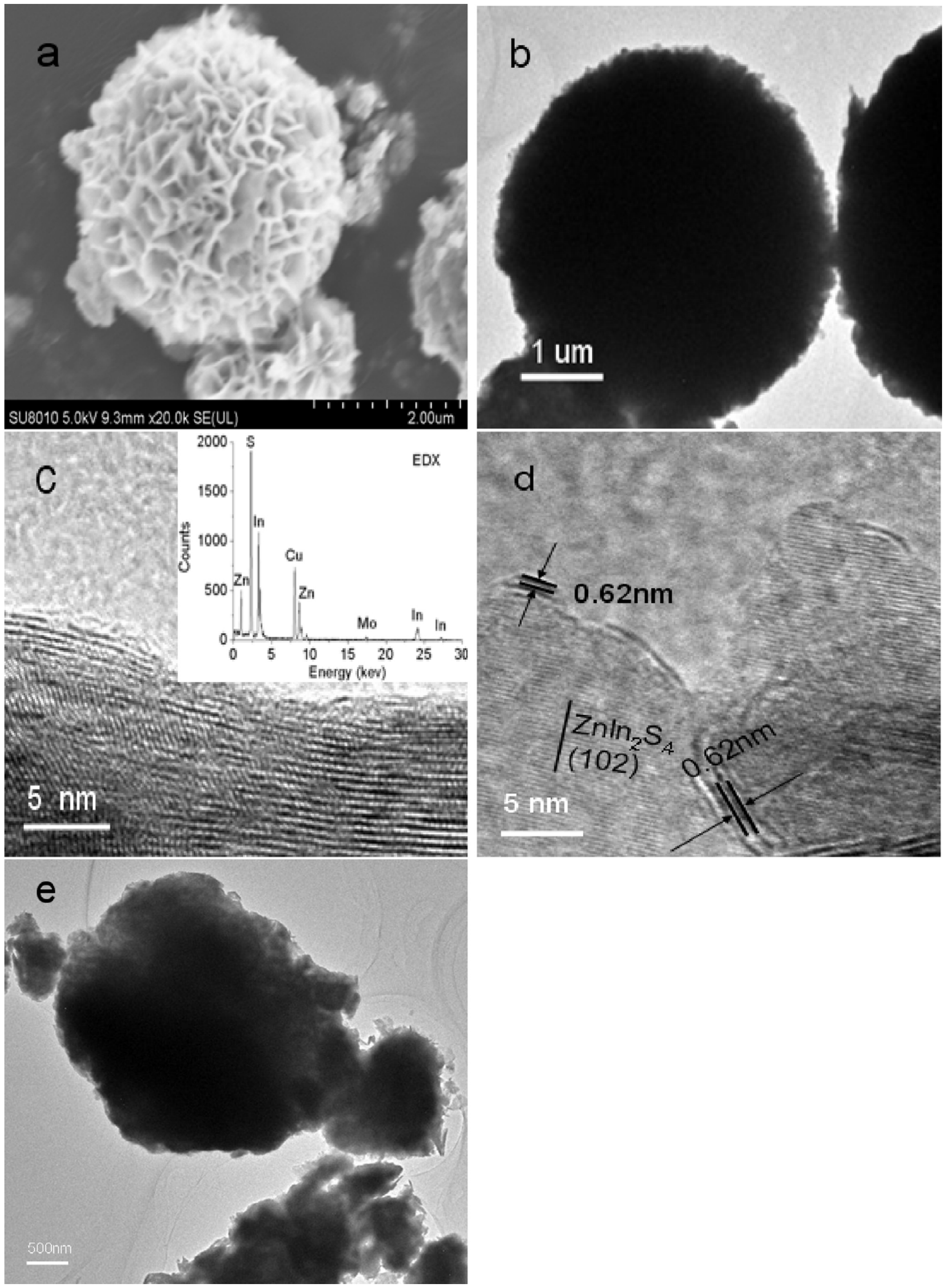

Fig. 4. MoS_2-$ZnIn_2S_4$-623 K (a) SEM image; (b) TEM image; (c) HRTEM image (inset: EDS); $MoS_2/ZnIn_2S_4$-723 K; (d) HRTEM image; (e) TEM image.

respectively, suggesting that Mo exist in the chemical states of Mo^{4+} (Fig. 3a). These values are close to those previously reported for MoS_2 [39,40]. The high resolution XPS spectra of S 2p region can be deconvoluted into two peaks at around 161.7 and 162.8 eV, which can be assigned to S^{2-} in $ZnIn_2S_4$ and MoS_2, respectively (Fig. 3b). As compared to the binding energy of Zn 2p observed over MoS_2-free $ZnIn_2S_4$ (1020.7 and 1043.6 eV), a higher binding energy shift was observed over $MoS_2/ZnIn_2S_4$ nanocomposite (1022.3 and 1045.2 eV) (Fig. 3c). Similar high binding energy shift has also been observed over the high resolution XPS spectra of In 3d (Fig. 3d). Such a shift to high binding energy may suggest a strong interaction between $ZnIn_2S_4$ and MoS_2. A decrease of the electron density of Zn^{2+} and In^{3+} in the $MoS_2/ZnIn_2S_4$ nanocomposite due to the electron transfer from $ZnIn_2S_4$ to the more electronegative MoS_2 when $ZnIn_2S_4$ are connected with MoS_2 may explain such a high binding energy shift.

The SEM and TEM images reveal that the $MoS_2/ZnIn_2S_4$-623 K nanocomposite was composed of microspheres with dimension in the range of 2–6 μm assembled by densely packed petals, indicating that the morphology of $ZnIn_2S_4$ was not significantly changed after the incorporation of MoS_2 (Fig. 4a and b). Although the HRTEM image does not show lattice fringes corresponding to MoS_2, the existence of Mo and S is evidenced from the energy-dispersive X-ray spectrometry (EDS), suggesting that MoS_2 existing in amorphous state in the as-prepared $MoS_2/ZnIn_2S_4$-623 K (Fig. 4c and inset). On the contrary, clear lattice fringe of 0.62 nm corresponding to the (0 0 2) plane of hexagonal MoS_2 can be observed on the HRTEM image of $MoS_2/ZnIn_2S_4$-723 K, indicating that amorphous MoS_2 gradually transform to crystalline MoS_2 at elevated temperature (Fig. 4d). However when calcinated at 723 K, the microspheres observed on the TEM image of $MoS_2/ZnIn_2S_4$-623 K were partially decomposed and aggregated (Fig. 4e).

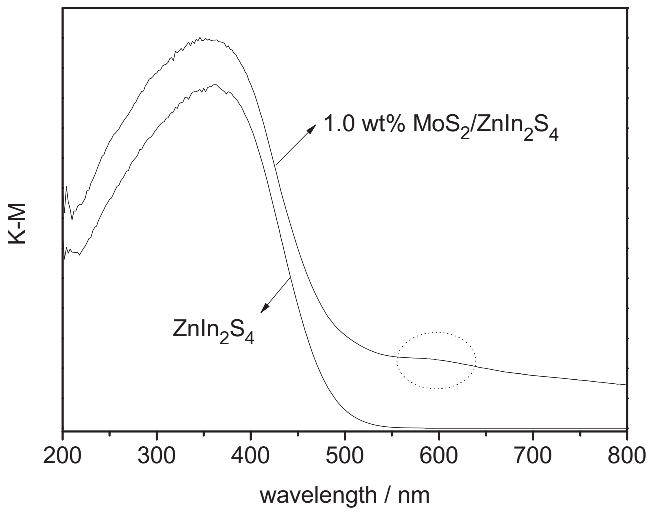

Fig. 5. UV–vis DRS of 1.0 wt% $MoS_2/ZnIn_2S_4$ and pure $ZnIn_2S_4$.

The UV–vis DRS of the $MoS_2/ZnIn_2S_4$ nanocomposite obtained at different temperature does not show much difference and a typical one was shown in Fig. 5. The UV–vis DRS of the $MoS_2/ZnIn_2S_4$ nanocomposite showed characteristic absorption corresponding to that of $ZnIn_2S_4$ and enhanced absorption in the region of 500–700 nm which can be ascribed to the absorption of MoS_2.

Photocatalytic hydrogen production experiments were carried out over the as-prepared $MoS_2/ZnIn_2S_4$ nanocomposites in the presence of Na_2S/Na_2SO_3 as sacrificial agent under visible light irradiations. Fig. 6 shows the hydrogen evolution rate for 1.0 wt% $MoS_2/ZnIn_2S_4$ nanocomposites obtained at different temperature and compared to that of pure $ZnIn_2S_4$ and MoS_2. No H_2 was detected when MoS_2 used as photocatalyst alone, suggesting that MoS_2 alone is not active for photocatalytic hydrogen evolution. In the absence of MoS_2, $ZnIn_2S_4$ only had a very low activity with the hydrogen evolution rate at 14.1 μmol/h. The hydrogen evolution rate over 1.0 wt% $MoS_2/ZnIn_2S_4$-623 K is significantly enhanced to 141 μmol/h, which is 10 times of that over bare $ZnIn_2S_4$ under similar condition. Although 1.0 wt% $MoS_2/ZnIn_2S_4$-723 K still showed a high photocatalytic activity for hydrogen evolution (70.8 μmol/h) as compared to bare $ZnIn_2S_4$, the increasing of the calcination temperature to 723 K in the preparation of $MoS_2/ZnIn_2S_4$ nanocomposite lead to a lower of its photocatalytic activity for hydrogen evolution. The lower photocatalytic hydrogen evolution observed

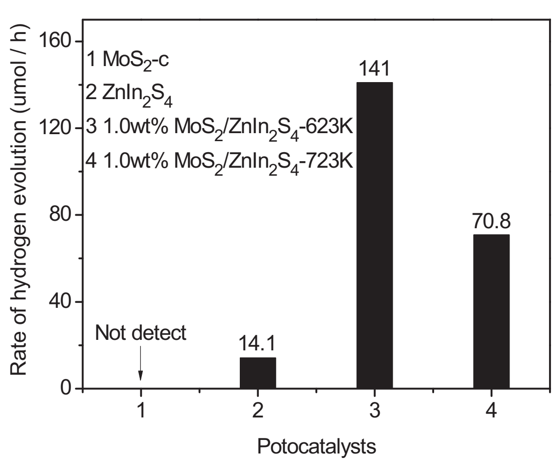

Fig. 6. Photocatalytic hydrogen evolution rate over (1) pure MoS_2; (2) pure $ZnIn_2S_4$; (3) 1.0 wt% $MoS_2/ZnIn_2S_4$-623 K and (4) 1.0 wt% $MoS_2/ZnIn_2S_4$-723 K (reaction conditions: catalyst, 0.05 g; 100 ml H_2O containing 0.43 M Na_2S and 0.5 M Na_2SO_3).

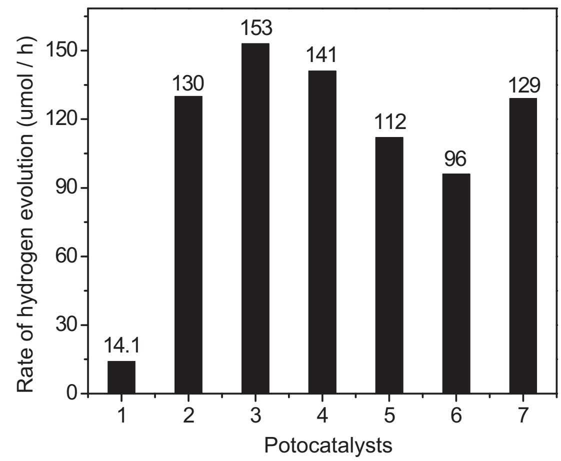

Fig. 7. Photocatalytic hydrogen evolution rate over (1) pure $ZnIn_2S_4$; $ZnIn_2S_4$ with different amounts of MoS_2 (2) 0.3 wt%; (3) 0.6 wt%; (4) 1.0 wt%; (5) 3.0 wt%; (6) 5.0 wt% and (7) 1.0 wt% Pt/$ZnIn_2S_4$ (reaction conditions: catalyst, 0.05 g; 100 ml H_2O containing 0.43 M Na_2S and 0.5 M Na_2SO_3).

over $MoS_2/ZnIn_2S_4$-723 K as compared to $MoS_2/ZnIn_2S_4$-623 K may be explained by the partial transformation of hexagonal $ZnIn_2S_4$ to rhombohedral one since it has already been well established that semiconductors with different polymorphs usually exhibit different photocatalytic activity.

Since the HRTEM image shows that MoS_2 in $MoS_2/ZnIn_2S_4$-623 K nanocomposite exists in amorphous state, while that in product obtained at 723 K is crystallized MoS_2, the current study indicates that even the amorphous MoS_2 can be excellent co-catalyst to promote the photocatalytic hydrogen evolution reaction. This is different from previous results since almost all the previous studies using MoS_2 as co-catalyst to promote the photocatalytic hydrogen evolution involves crystalline MoS_2 instead of amorphous one. However, the promoting effect on the photocatalytic hydrogen evolution played by the amorphous MoS_2 is not so surprising since amorphous MoS_2 have already been demonstrated to show excellent HER activity. Previous DFT studies on MoS_2 reveals that Mo $(10\bar{1}0)$ edge sites with 50% S adsorption are active for HER because the adsorbed sulfur atoms at the edge sites are unsaturated and can act as the adsorption site for H atoms [31]. Although the amorphous MoS_2 lacks such well-defined Mo $(10\bar{1}0)$ edge sites, there exists many defect sites in the amorphous MoS_2. These defect sites possess many coordinately and structurally unsaturated sulfur atoms, which also can act as adsorption site for hydrogen atoms and eventually leads to hydrogen evolution [41]. Our current result demonstrated that as that observed over MoS_2 for HER, amorphous MoS_2 can also show excellent promoting effect for photocatalytic hydrogen evolution.

The effect of MoS_2 loading amount on the photocatalytic hydrogen evolution is also investigated. Fig. 7 shows that the photocatalytic hydrogen evolution rate over $MoS_2/ZnIn_2S_4$-623 K loaded with different amounts of MoS_2. It shows that the introduction of only a little amount of MoS_2 (0.3 wt%) can significantly increase the hydrogen evolution rate to 130 μmol/h, an almost 9.3 times as that over bare $ZnIn_2S_4$ (14.1 μmol/h). An optimum MoS_2 loading amount is found at 0.6 wt%, which exhibit the highest photocatalytic hydrogen evolution rate of 153 μmol/h. This value is much higher than that observed over 1.0 wt% Pt/$ZnIn_2S_4$ nanocomposite (129 μmol/h). A further increase in the amount of MoS_2 results in a decrease in the photocatalytic hydrogen evolution rate. Such a decrease in the activity of samples with a heavy loading of MoS_2 is likely due to the shading effect of MoS_2, which can block the absorption of the incident light by $ZnIn_2S_4$.

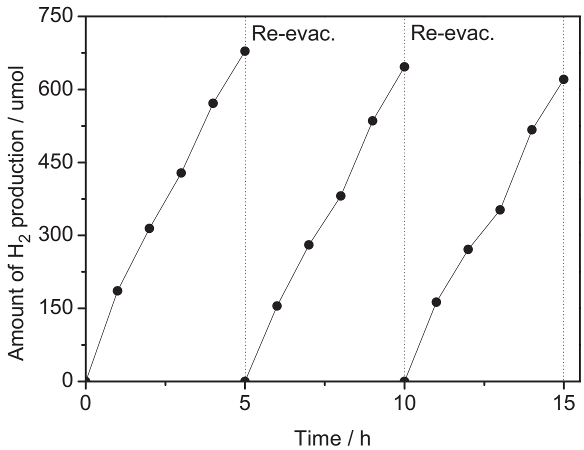

Fig. 8. Amount of hydrogen evolved over 1.0 wt% $MoS_2/ZnIn_2S_4$-623 K system in a 15 h photocatalytic reaction (reaction conditions: catalyst, 0.05 g; 100 ml H_2O containing 0.43 M Na_2S and 0.5 M Na_2SO_3).

The stability of $MoS_2/ZnIn_2S_4$ during the photocatalytic reaction was confirmed by the XRD of the photocatalyst after the reaction (supporting information Fig. S1). In addition to this, a prolonged photocatalytic reaction in 15 h revealed that no obvious loss of the activity during the whole reaction period, another confirmation of the stability of $MoS_2/ZnIn_2S_4$ during the photocatalytic hydrogen evolution (Fig. 8).

Scheme 1 shows the mechanism proposed for the enhanced hydrogen evolution over $MoS_2/ZnIn_2S_4$ nanocomposite. Since the conduction band of MoS_2 is less negative than that of hexagonal $ZnIn_2S_4$, a directional transfer of the photogenerated electrons from $ZnIn_2S_4$ to MoS_2 is feasible. In addition to this, the electrons transferred to the conduction band of MoS_2 exhibit enough redox potential to reduce H^+ to produce hydrogen at HER active sites of MoS_2, while the holes left in $ZnIn_2S_4$ can oxidize the sacrificial agent. Controlled experiment performed on a mixture of $ZnIn_2S_4$ and MoS_2 under similar reaction condition revealed that the photocatalytic performance of $ZnIn_2S_4$ can also be enhanced. However, the rate for hydrogen evolution over a mechanical mixture of $ZnIn_2S_4$ and MoS_2 (53.7 μmol/h) is much smaller than that observed over $MoS_2/ZnIn_2S_4$ nanocomposite (Supporting materials Table S1). Due to their analogous intrinsic layered structures, the formation of a good junction between $ZnIn_2S_4$ and MoS_2 is believed to benefit the directional migration of the photo-excited electrons from $ZnIn_2S_4$ to MoS_2, which lead to a highly enhanced photocatalytic performance for hydrogen evolution over $MoS_2/ZnIn_2S_4$ nanocomposites.

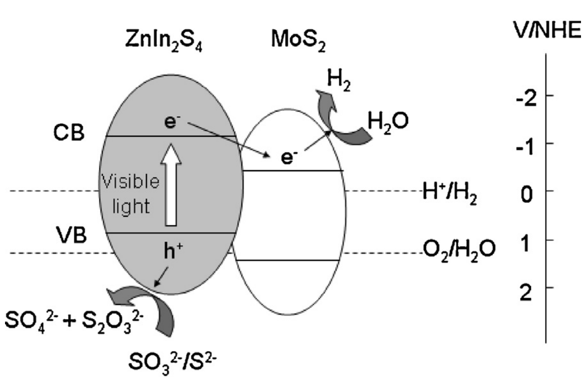

Scheme 1. Proposed mechanism for photocatalytic hydrogen evolution over $MoS_2/ZnIn_2S_4$ nanocomposite under visible light irradiations.

4. Conclusion

In summary, $MoS_2/ZnIn_2S_4$ nanocomposites prepared by impregnating hexagonal $ZnIn_2S_4$ with $(NH_4)_2MoS_4$, followed by a treatment in H_2S flow at high temperatures showed highly enhanced photocatalytic performance for hydrogen evolution under visible light irradiations. The photocatalytic activity of $MoS_2/ZnIn_2S_4$ nanocomposites can be even higher than that of $Pt/ZnIn_2S_4$. Due to the existence of many defect sites which act as adsorption site for hydrogen atoms and eventually leads to hydrogen evolution, amorphous MoS_2 was shown for the first time to exhibit excellent promoting effect for photocatalytic hydrogen evolution. This work demonstrates a high potential of developing the environmental friendly, cheap non-noble-metal co-catalyst for semiconductor-based photocatalytic hydrogen evolution.

Acknowledgments

The work was supported by NSFC (21273035, J1103303), 973 Programs (2014CB239303, 2011CB612314 and 2013CB632405) and Specialized Research Fund for the Doctoral Program of Higher Education (20123514110002). Z. Li thanks the Award Program for Minjiang Scholar Professorship for financial support.

Appendix A. Supplementary data

Supplementary data associated with this article can be found, in the online version, at http://dx.doi.org/10.1016/j.apcatb.2013.07.064.

References

[1] J.A. Turner, Science 305 (2004) 972–974.
[2] N.S. Lewis, D.G. Nocera, Proceedings of the National Academy of Sciences of the United States of America 103 (2006) 15729–15735.
[3] H. Tong, S.X. Ouyang, Y.P. Bi, N. Umezawa, M. Oshikiri, J.H. Ye, Advanced Materials 24 (2012) 229–251.
[4] X.B. Chen, S.H. Shen, L.J. Guo, S.S. Mao, Chemical Reviews 110 (2010) 6503–6570.
[5] A. Fujishima, K. Honda, Nature 238 (1972) 37–38.
[6] W.J. Ren, Z.H. Ai, F.L. Jia, L.Z. Zhang, X.X. Fan, Z.G. Zou, Applied Catalysis B: Environmental 69 (2007) 138–144.
[7] Y.F. Wang, M.C. Hsieh, J.F. Lee, C.M. Yang, Applied Catalysis B: Environmental 142/143 (2013) 626–632.
[8] M. Altomare, M. Pozzi, M. Allieta, L.G. Bettini, El. Selli, Applied Catalysis B: Environmental 136/137 (2013) 81–88.
[9] Q.J. Xiang, B. Cheng, J.G. Yu, Applied Catalysis B: Environmental 138/139 (2013) 299–303.
[10] I. Tsuji, H. Kato, H. Kobayashi, A. Kudo, Journal of the American Chemical Society 126 (2004) 13406–13414.
[11] W.J. Luo, Z.S. Li, X.J. Jiang, T. Yu, L.F. Liu, X.Y. Chen, J.H. Ye, Z.G. Zou, Physical Chemistry Chemical Physics 10 (2008) 6717–6723.
[12] R. Sasaki, K. Maeda, Y. Kako, K. Domen, Applied Catalysis B: Environmental 128 (2012) 72–76.
[13] Z.B. Lei, W.S. You, M.Y. Liu, G.H. Zhou, T. Takata, M. Hara, K. Domen, C. Li, Chemical Communications 17 (2003) 2142–2143.
[14] Y.J. Chen, S.W. Hu, W.J. Liu, X.Y. Chen, L. Wu, X.X. Wang, P. Liu, Z.H. Li, Dalton Transactions 40 (2011) 2607–2613.
[15] S.H. Shen, L. Zhao, L.J. Guo, International Journal of Hydrogen Energy 33 (2008) 4501–4510.
[16] B. Chai, T.Y. Peng, P. Zeng, X. Zhang, X.J. Liu, Journal of Physical Chemistry C 115 (2011) 6149–6155.
[17] I. Tsuji, H. Kato, H. Kobayashi, A. Kudo, Chemistry of Materials 18 (2006) 1969–1975.
[18] H. Kominami, H. Nishimune, Y. Ohta, Y. Arakawa, T. Inaba, Applied Catalysis B: Environmental 111/112 (2012) 297–302.
[19] B. Pal, T. Torimoto, K. Okazaki, B. Ohtani, Chemical Communications 5 (2007) 483–485.
[20] P.C. Shen, S. Zhao, D. Su, Y. Li, A. Orlov, Applied Catalysis B: Environmental 126 (2012) 153–160.
[21] S.S. Rayalu, D. Jose, M.V. Joshi, P.A. Mangrulkar, K. Shrestha, K. Klabunde, Applied Catalysis B: Environmental 142/143 (2013) 684–693.
[22] H. Yuzawa, T. Yoshida, H. Yoshida, Applied Catalysis B: Environmental 115/116 (2012) 294–302.
[23] D. Chen, J.H. Ye, Chemistry of Materials 21 (2009) 2327–2333.
[24] T. Takata, K. Domen, Journal of Physical Chemistry C 113 (2009) 19386–19388.

[25] X. Zong, H.J. Yan, G.P. Wu, G.J. Ma, F.Y. Wen, L. Wang, C. Li, Journal of the American Chemical Society 130 (2008) 7176–7177.
[26] G.P. Chen, D.M. Li, F. Li, Y.Z. Fan, H.F. Zhao, Y.H. Luo, R.C. Yu, Q.B. Meng, Applied Catalysis A: General 443/444 (2012) 138–144.
[27] S. Kanda, T. Akita, M. Fujishima, H. Tada, Journal of Colloid and Interface Science 354 (2011) 607–610.
[28] Q.J. Xiang, J.G. Yu, M. Jaroniec, Journal of the American Chemical Society 134 (2012) 6575–6578.
[29] X. Zong, J.F. Han, G.J. Ma, H.J. Yan, J.P. Wu, C. Li, Journal of Physical Chemistry C 115 (2011) 12202–12208.
[30] W. Zhang, Y.B. Wang, Z. Wang, Z.Y. Zhong, R. Xu, Chemical Communications 46 (2010) 7631–7633.
[31] B. Hinnemann, P.G. Moses, J. Bonde, K.P. Jørgensen, J.H. Nielsen, S. Horch, I. Chorkendorff, J.K. Nørskov, Journal of the American Chemical Society 127 (2005) 5308–5309.
[32] Y.G. Li, H.L. Wang, L.M. Xie, Y.Y. Liang, G.S. Hong, H.J. Dai, Journal of the American Chemical Society 133 (2011) 7296–7299.
[33] Y.D. Hou, A.B. Laursen, J.S. Zhang, G.G. Zhang, Y.S. Zhu, X.C. Wang, S. Dahl, I. Chorkendorff, Angewandte Chemie International Edition 52 (2013) 1–6.
[34] T.R. Thurston, J.P. Wilcoxon, Journal of Physical Chemistry B 103 (1999) 11–17.
[35] D. Genuit, P. Afanasiev, M. Vrinat, Journal of Catalysis 235 (2005) 302–317.
[36] S.J. Sandoval, D. Yang, R.F. Frindt, J.C. Irwin, Physical Review B 44 (1991) 3955–3962.
[37] Z.Y. Zeng, Z.Y. Yin, X. Huang, H. Li, Q.Y. He, G. Lu, F. Boey, H. Zhang, Angewandte Chemie International Edition 50 (2011) 11093–11097.
[38] H.S.S. Ramakrishna Matte, A. Gomathi, A.K. Manna, D.J. Late, R. Datta, S.K. Pati, C.N.R. Rao, Angewandte Chemie International Edition 49 (2010) 4059–4062.
[39] B.A. Vanchura, P.G. He, V. Antochshuk, M. Jaroniec, A. Ferryman, D. Barbash, J.E. Fulghum, S.D. Huang, Journal of the American Chemical Society 124 (2002) 12090–12091.
[40] W.K. Ho, J.C. Yu, J. Lin, J.G. Yu, P.S. Li, Langmuir 20 (2004) 5865–5869.
[41] D. Merki, X.L. Hu, Energy & Environmental Science 4 (2011) 3878–3888.